Geophysical Research Letters

RESEARCH LETTER
10.1029/2022GL099325

Tropical Instability Waves and Wind-Forced Cross-Equatorial Flow in the Central Atlantic Ocean

Finn Ole Heukamp[1], Peter Brandt[2,3], Marcus Dengler[2], Franz Philip Tuchen[4], Michael J. McPhaden[5], and James N. Moum[6]

[1]Alfred-Wegener-Institute, Helmholtz Centre for Polar and Marine Research, Bremerhaven, Germany, [2]GEOMAR Helmholtz Centre for Ocean Research Kiel, Kiel, Germany, [3]Christian-Albrechts-Universität zu Kiel, Kiel, Germany, [4]NOAA/Atlantic Oceanographic and Meteorological Laboratory, Miami, FL, USA, [5]NOAA Pacific Marine Environmental Laboratory, Seattle, WA, USA, [6]College of Earth, Ocean, and Atmospheric Sciences, Oregon State University, Corvallis, OR, USA

Abstract Based on velocity data from a long-term moored observatory located at 0°N, 23°W we present evidence of a vertical asymmetry during the intraseasonal maxima of northward and southward upper-ocean flow in the equatorial Atlantic Ocean. Periods of northward flow are characterized by a meridional velocity maximum close to the surface, while southward phases show a subsurface velocity maximum at about 40 m. We show that the observed asymmetry is caused by the local winds. Southerly wind stress at the equator drives northward flow near the surface and southward flow below that is superimposed on the Tropical Instability Wave (TIW) velocity field. This wind-driven overturning cell, known as the Equatorial Roll, shows a distinct seasonal cycle linked to the seasonality of the meridional component of the south-easterly trade winds. The superposition of vertical shear of the Equatorial Roll and TIWs causes asymmetric mixing during northward and southward TIW phases.

Plain Language Summary Tropical Instability Waves (TIWs) are clear in satellite measurements of sea surface temperature as horizontal undulations with wavelength of the order of 1,000 km in equatorial regions of both Atlantic and Pacific Oceans. TIWs are characterized by their distinctive upper-ocean meridional velocity structure. TIWs amplify vertical shear and thus contribute to the generation of turbulence which in turn leads to the mixing of heat and freshwater downward into the deeper ocean. In this study we show that the prevailing southerly winds in the central equatorial Atlantic drive near-surface northward and subsurface southward flows, which are superposed on the meridional TIW velocity field. The strength of this wind driven cell is linked to the seasonal cycle of the northward component of the trade winds, peaking in boreal fall when TIWs reach their maximum amplitude. The overturning cell affects the vertical structure of the meridional velocity field and thus has impact on the generation of current shear and turbulence. We show that the overturning reduces/enhances shear during northward/southward TIW flow, an asymmetry that is consistent with independent measurements showing asymmetric mixing.

Key Points:

- Composites of Tropical Instability Waves at 0°N, 23°W show a surface (subsurface) velocity maximum during northward (southward) phases
- Meridional wind stress forces a seasonally-varying, shallow cross-equatorial overturning cell-the Equatorial Roll
- The superposition of Tropical Instability Waves and Equatorial Roll causes asymmetric mixing during north- and southward phases

Supporting Information:

Supporting Information may be found in the online version of this article.

Correspondence to:

F. O. Heukamp,
Finn.Heukamp@awi.de

Citation:

Heukamp, F. O., Brandt, P., Dengler, M., Tuchen, F. P., McPhaden, M. J., & Moum, J. N. (2022). Tropical instability waves and wind-forced cross-equatorial flow in the Central Atlantic Ocean. *Geophysical Research Letters*, *49*, e2022GL099325. https://doi.org/10.1029/2022GL099325

Received 4 MAY 2022
Accepted 2 SEP 2022

Author Contributions:

Conceptualization: Finn Ole Heukamp, Peter Brandt, Marcus Dengler
Data curation: Peter Brandt, Marcus Dengler, Franz Philip Tuchen, Michael J. McPhaden, James N. Moum
Formal analysis: Finn Ole Heukamp
Investigation: Finn Ole Heukamp, Peter Brandt, Marcus Dengler
Methodology: Finn Ole Heukamp, Peter Brandt, Marcus Dengler, Franz Philip Tuchen, Michael J. McPhaden, James N. Moum
Software: Finn Ole Heukamp
Supervision: Peter Brandt, Marcus Dengler

1. Introduction

The mean circulation in the central tropical Atlantic Ocean is dominated by vigorous zonal currents (Brandt et al., 2006). At the equator, the most prominent currents are the Equatorial Undercurrent (EUC) flowing eastwards at thermocline level, bounded by the different branches of the westward flowing South Equatorial Current (SEC). These are the northern SEC (nSEC) at 2°N and the central SEC (cSEC) at 4°S. Mean surface flow at the equator is westward as well, leading to substantial vertical shear at the equator (Hummels et al., 2013). The seasonal variability of the equatorial current system is in large part controlled by the direction and strength of the trade winds that are tightly linked to the annual migration of the Intertropical Convergence Zone (ITCZ). During the northward migration of the ITCZ in boreal spring/early summer, the westward component of the southeast trade winds intensifies and accelerates the nSEC and the eastward North Equatorial Counter Current (NECC) (Grodsky et al., 2003, 2005). In turn, the intense meridional shear of zonal velocity between the EUC, nSEC, and NECC during boreal summer leads to barotropic shear instabilities generating Tropical Instability Waves (TIWs) (Grodsky et al., 2005; Jochum et al., 2004; Kelly et al., 1995; Perez et al., 2019). Additionally, baroclinic instabilities associated with the intensified zonal current system contribute to TIW generation (McCreary & Yu, 1992; von Schuckmann et al., 2008). The vertical structure of TIWs as obtained from cruises in the equatorial Pacific revealed vertical asymmetries in the TIW velocity field with surface-intensified northward

Validation: Finn Ole Heukamp, Peter Brandt, Marcus Dengler
Visualization: Finn Ole Heukamp
Writing – original draft: Finn Ole Heukamp
Writing – review & editing: Finn Ole Heukamp, Peter Brandt, Marcus Dengler, Franz Philip Tuchen, Michael J. McPhaden, James N. Moum

and subsurface-intensified southward flow along 4°N, but suggested symmetric flow directly on the equator (Kennan & Flament, 2000).

TIWs add vertical shear of meridional velocity to the total vertical shear, which is typically dominated by the vertical shear of zonal velocity above the core of the EUC, thereby intensifying diapycnal mixing (Hummels et al., 2013; Inoue et al., 2019; Moum et al., 2009). To explain variations in the TIW-induced mixing, Holmes and Thomas (2015) suggested vortex stretching and enhanced shear of the EUC flow at the leading edge of TIW warm phases at the equator. Liu et al. (2019) and Specht et al. (2021) further reported on the existence of subsurface-intensified TIWs at the equator that primarily manifest in zonal velocities with maximum amplitudes at 70–90 m in the Pacific Ocean and 30–90 m in the Atlantic Ocean, leading to complex shear and diapycnal mixing structures.

The impact of the wind on the equatorial flow field is, however, not limited to the forcing of zonal currents and can drive cross-equatorial flow. Mayer and Weisberg (1993) showed that the wind curl at the equator in the Atlantic Ocean drives an interior southward cross-equatorial Sverdrup flow responsible for the establishment of an equatorial gyre (e.g., Fratantoni et al., 2000). Moreover, Perez et al. (2014) presented long-term time-mean meridional sections along 23°W that reveal tropical cells (TC) north and south of the equator with near-surface poleward and subsurface equatorward flow driven by the winds. The northern TC expands across the equator, resulting in northward flow above ∼30 m depth and southward flow below down to ∼100 m at the equator, indicating the existence of a shallow cross-equatorial overturning cell, a feature that was first described in the Indian Ocean (Miyama et al., 2003; Schott et al., 2002; Wacongne & Pacanowski, 1996; Wang & McPhaden, 2017) and is referred to as the Equatorial Roll (ER). Particularly during September/October southerly winds prevail at the equator. These winds turn northeastward north of the equator associated with the establishment of the West African Monsoon, thus the situation in the equatorial Atlantic resembles very closely that of the Indian Ocean mean wind field (Schott et al., 2009).

With the present study we aim to investigate mean characteristics of TIW associated meridional velocity fields in the central equatorial Atlantic. We will differentiate between north-/southward TIW phases that are defined without subtracting the climatology of meridional velocity. We attribute the enhanced vertical shear of meridional velocity during southward TIW phases to the superposition of TIWs and the wind-forced meridional circulation.

2. Data

Approximately 20 years of current velocity data (Tuchen et al., 2022) from a moored observatory that is part of the Prediction and Research Moored Array in the Tropical Atlantic (PIRATA) (Bourlès et al., 2019) at 0°N, 23°W are investigated in this study. To reduce short period variability, a 48-hr boxcar window was applied to the data set. Due to gaps in the data, we only consider data with coverage of at least 75% in the upper 75 m (Figure S1 in Supporting Information S1). Moreover, we make use of daily mean wind speed recorded at the PIRATA buoy between 2001 and 2021 as well as a wind stress curl climatology from Risien and Chelton (2008). Further, daily mean χ-pod turbulence data (Moum et al., 2022, Text S1 in Supporting Information S1) from the mooring site are investigated.

3. Upper Ocean Meridional Velocity Fluctuations at 0°N, 23°W

In contrast to the rather slowly-varying zonal current system in the equatorial Atlantic, with westward surface velocities of the nSEC and eastward flow at thermocline level by the EUC (e.g., Brandt et al., 2021), the meridional velocity recorded at the 0°N, 23°W mooring site is dominated by intraseasonal variability with periods of 18–50 days (Figures 1a and 1b). First, we will focus on meridional velocity fluctuations averaged between the uppermost available velocity records and 75 m. The derived fluctuations are a manifestation of TIWs, a continuous band of wave-like structures passing the mooring site from east to west, thereby changing the flow direction from northward in the leading phase of a TIW to southward in the subsequent phase. The moored velocity records show that the amplitude of the meridional velocity fluctuations undergoes a distinct seasonal cycle (Körner et al., 2022; Tuchen et al., 2018) with increasing amplitudes during boreal spring and early summer, maximum velocities occasionally exceeding 50 cm/s in boreal summer and early fall before decreasing again in late boreal fall and winter. Despite the seasonality, the record also reveals strong year-to-year variability in the strength and occurrence of TIWs.

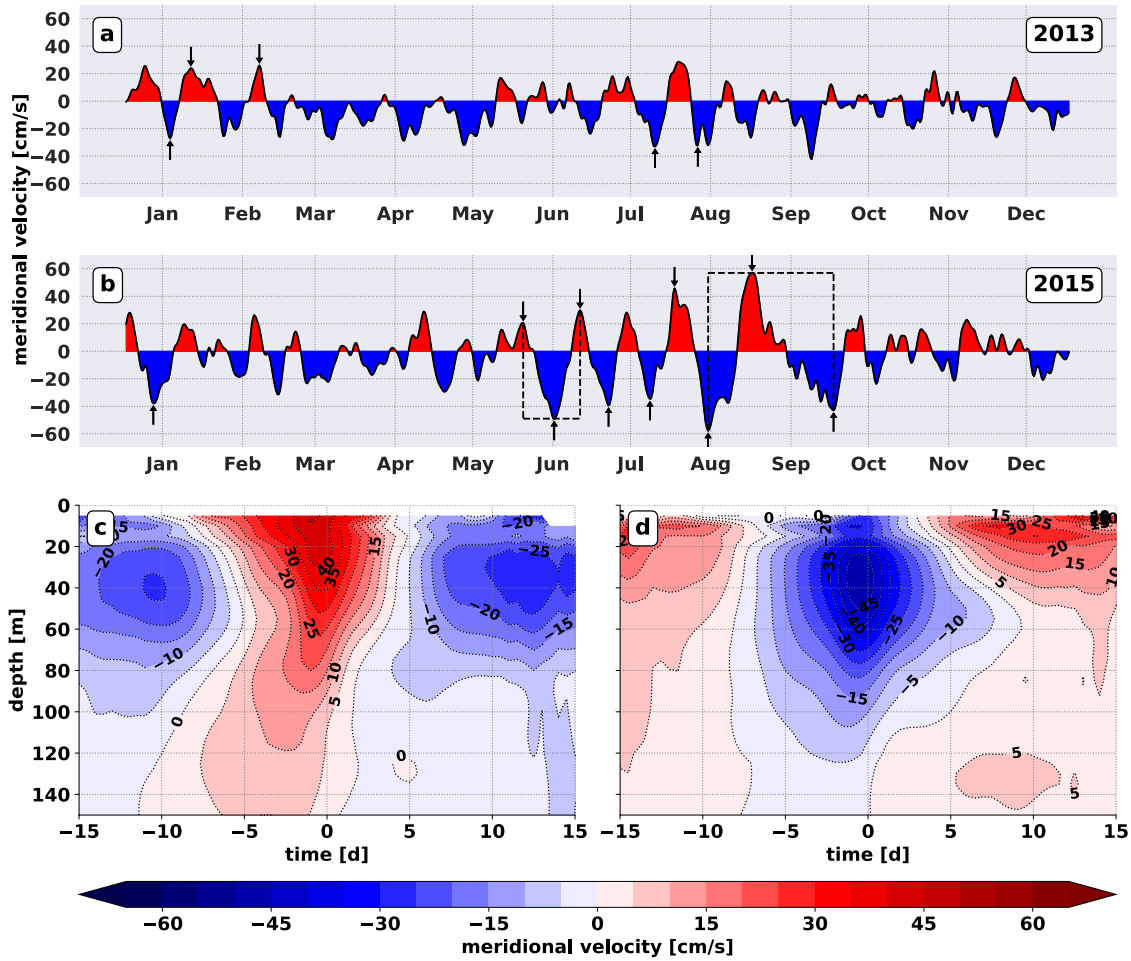

Figure 1. Mooring record of mean 0–75 m meridional velocities at 0°N, 23°W for (a) 2013 and (b) 2015. Black arrows in (a) and (b) denote flow phases that are identified as tropical instability waves (TIW) phases. Tick marks denote the center of the month. Dashed black lines indicate the amplitude and duration criteria for two cases. Depth-time composites of meridional velocities of (c) northward and (d) southward TIW phases from 2001 to 2021 centered at their corresponding maximum mean 0–75 m meridional velocities. Only the 40 strongest TIW peaks of each phase are considered. Note that the meridional velocity climatology is not subtracted.

In 2015, the seasonal cycle in the magnitude of TIW associated velocities was well established with pronounced meridional velocity fluctuations in boreal summer (Figure 1b). However, in other years, as for instance 2013, hardly any seasonal intensification is observed and meridional velocity amplitudes rarely exceed 20 cm/s (Figure 1a). Independent of the strength of the seasonal cycle, these 2 years generally indicate events of enhanced southward velocities to outlast and exceed events of enhanced northward flow in terms of duration and amplitude. To account for this asymmetry, we apply a specific method to detect northward and southward flow phases in the mean 0–75 m meridional velocity that we attribute to the passage of TIWs. For instance, a northward velocity peak is considered part of a TIW if

$$\frac{|A_1| + |A_2|}{2} > 40\,\mathrm{cm/s} \tag{1}$$

where A_1 (A_2) denotes the difference of the maximum northward flow of the considered velocity peak and the maximum velocity of the previous (subsequent) southward flow phase. Further, we only consider velocity peaks that fulfill a duration criterion following the observed intraseasonal peak of meridional velocity variability shown by Tuchen et al. (2018).

$$18\,\mathrm{days} \leq T(P_S) - T(P_P) \leq 50\,\mathrm{days} \tag{2}$$

where $T(P_S)$ ($T(P_P)$) denotes the time of the occurrence of the subsequent (previous) southward velocity peak. The same method is applied to the southward velocity peaks. The application of these criteria is visualized for

two example cases by the dashed black lines in Figure 1b. By applying this method, 60 northward TIW phases and 68 southward TIW phases were identified during the whole measurement period from 2001 to 2021 of which we choose the 40 northward and 40 southward phases with the largest amplitudes (Equation 1) for further investigation.

To compare the peak amplitude and duration of northward and southward TIW phases, all 40 identified northward/southward TIW phases were separated and centered at their maximum velocity. We find that the mean peak amplitude of southward TIW phases is larger and the southward flow lasts longer (-39 ± 9 cm/s, 16.5 ± 7 days) than the corresponding means of all northward TIW phases (31 ± 11 cm/s, 10.5 ± 5 days). The uncertainty given here represents one standard deviation.

In order to understand the dominance of southward TIW phases, we further expand our investigation toward the vertical, yielding depth-time composites of northward/southward TIW phases shown in Figures 1c and 1d. The meridional velocity composites of maximum northward and southward flow phases at the equator reveal remarkable differences in their vertical structure. While the northward flow steadily increases toward the surface (Figure 1c), the flow of the southward phase peaks at 40 m and then decreases toward the surface (Figure 1d). Moreover, duration of northward flow is longest close to the surface while southward flow duration is longest at about 50 m depth. The difference in the vertical structure is consistent with the imbalances found in the mean strength and duration of northward/southward TIW phases (Figures 1a and 1b). Since measurements shallower than 20 m are underrepresented in our data set, the 0–75 m mean meridional velocity is biased by an overrepresentation of the strong southward, subsurface flow compared to the northward near-surface maximum of northward TIW phases.

Although the cause of the imbalance in mean peak amplitude and duration can largely be attributed to the sparse data coverage near the surface, the asymmetry in the vertical structure of northward and southward TIW phases has not yet been described and is unexpected given that, for example, TIWs in the equatorial Pacific were observed to be symmetric (Kennant & Flament, 2000).

To further investigate the difference in the vertical structure, we turn our attention to the impact of the prevailing southerly winds in the equatorial Atlantic.

4. Impact of Meridional Winds on Upper Ocean Velocities in the Equatorial Atlantic

The surface wind in the equatorial Atlantic is dominated by southeast trade winds as the mean position of the ITCZ is located north of the equator. Hence, the southeast trades crossing the equator result in a northward wind component at the equator on average. Superimposed on the mean wind field is a pronounced seasonal cycle associated with the seasonal migration of the ITCZ. During late boreal summer, the ITCZ is at its northernmost position. During that time of the year, south of the equator, southeast trades prevail, while on the equator, the winds turn northward and north-northeastward further north. The meridional wind component and the absence of the Coriolis force close to the equator provide reasonable conditions for the development of the Atlantic Equatorial Roll (ER). In order to assess the characteristics of the ER and its impact on the equatorial Atlantic circulation, a linear lead-lag regression analysis was applied to daily mean upper-ocean meridional velocity and meridional wind stress, $\boldsymbol{\tau_y}$ that is derived from PIRATA wind speed measurements:

$$\boldsymbol{\tau_y = \rho_{air} * c_d * \mid \vec{u}_{10} \mid * v_{10}}$$

where $\boldsymbol{\rho_{air} = 1.22\,kg\,m^{-3}}$ is the air density, $\boldsymbol{c_d = 0.0013}$ the drag coefficient, $\boldsymbol{\vec{u}_{10}}$ the wind speed vector, and $\boldsymbol{v_{10}}$ the meridional wind component. Here, we assume PIRATA winds measured at 4 m height equal winds at 10 m height.

Despite the elevated variability, regression analysis for different depths (Figure 2) suggests the existence of a shallow, wind-driven baroclinic response of the meridional flow reaching as deep as 80 m at the mooring site. As already pointed out, the availability of near-surface velocity data is sparse and largely limited to an enhanced monitoring period (Wenegrat et al., 2014; Wenegrat & McPhaden, 2015) and single-point current meter data at 10–12 m depth (Tuchen et al., 2022). However, even this limited data set reveals a strong positive regression coefficient of $\boldsymbol{\left(3.51 \pm 1.13\,m^3\,N^{-1}s^{-1}\right)}$ between meridional wind stress and meridional current velocity at 5 m depth (Figure 2a). Positive regression coefficients persist down to 20 m depth, but are substantially weakened compared

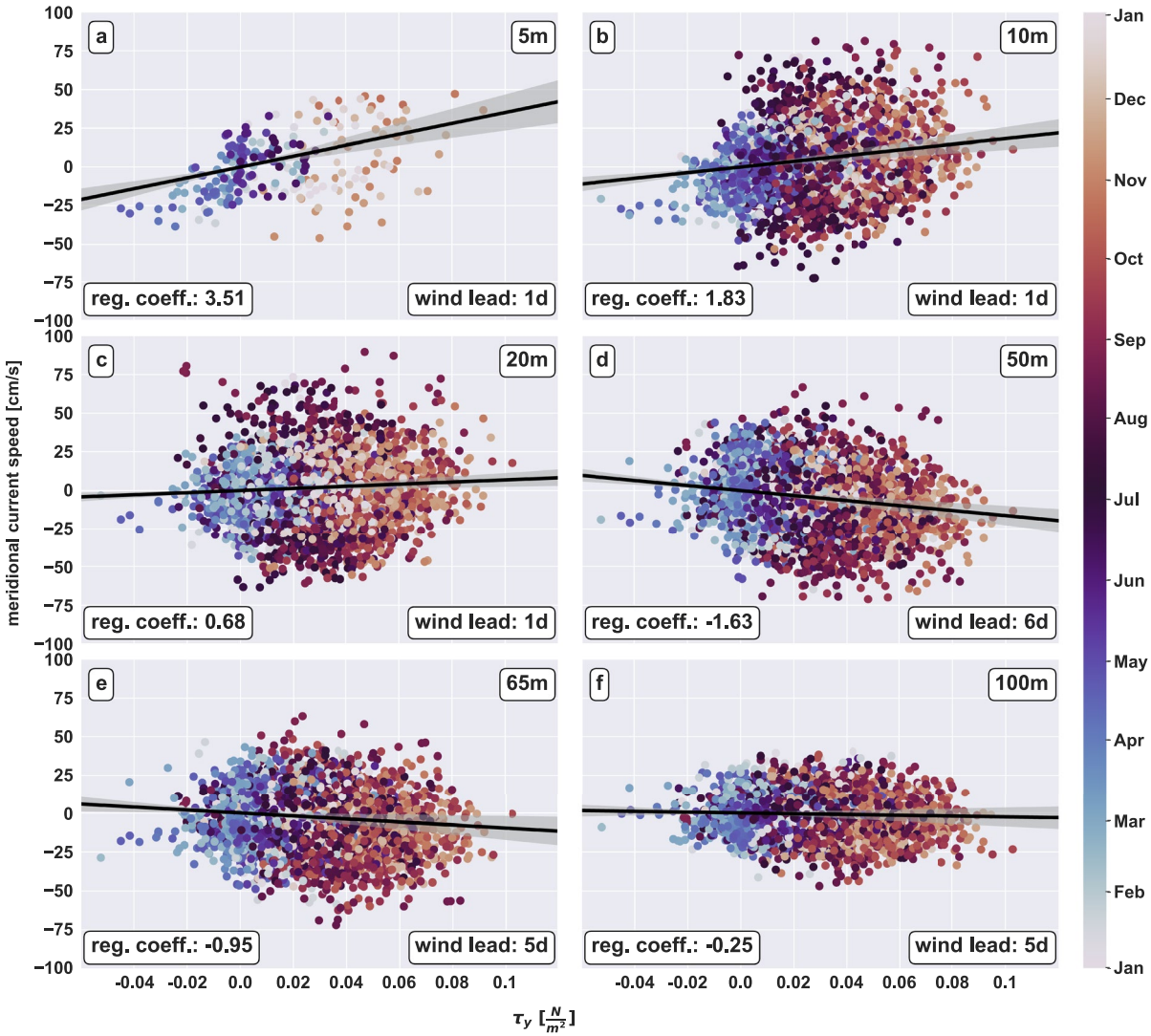

Figure 2. Scatter plots and regression analysis of daily mean meridional wind stress and meridional current speed at 0°N, 23°W for the whole measurement period from 2001 to 2021. To account for autocorrelation, uncertainties are computed as 95% confidence intervals of regression coefficients performed with a low-pass filtered and subsampled data set (details given in Figure S2 in Supporting Information S1). Unit of regression coefficients: $\frac{m}{s} \cdot \left(\frac{N}{m^2}\right)^{-1}$.

to the 5 m value. In the upper 20 m, maximum regression coefficients are found with 1 day wind lead time, indicating an almost instantaneous response of the near-surface velocity to changes in the meridional wind field (Figure 2a, 2b and 2c). In the deeper water column, the slope of the regression line turns negative and reaches its maximum at 50 m depth $\left(\mathbf{-1.63 \pm 0.59\ m^3\ N^{-1} s^{-1}}\right)$ (Figure 2d). The now inverse relation weakens further down to 65 m $\left(\mathbf{-0.95 \pm 0.73\,m^3\ N^{-1} s^{-1}}\right)$ before finally fading out (Figures 2e and 2f). Enhanced negative regression coefficients between 25 and 80 m are found at wind-lead-times between 5 and 6 days (Figures 2c–2e, Figure S2 in Supporting Information S1). Hence, in contrast to the instantaneous response of the meridional velocity in the near-surface layer to changes in the meridional wind stress, the maximum subsurface flow is delayed. Calculating this relation for low-/high-pass filtered wind-stress and velocity data indicates, despite differing amplitudes and phase lags, a consistent vertical structure from daily to seasonal timescales (Figure S2 in Supporting Information S1).

The vertical profile of the regression coefficients constructed from the maximum lead-lag regression coefficient at each depth level (Figure S2a in Supporting Information S1) and the climatological monthly mean meridional wind stress are further used to derive a climatology of the ER meridional flow, that is shown together with the meridional wind stress climatology as well as wind stress curl in Figure 3. Missing values in the regression

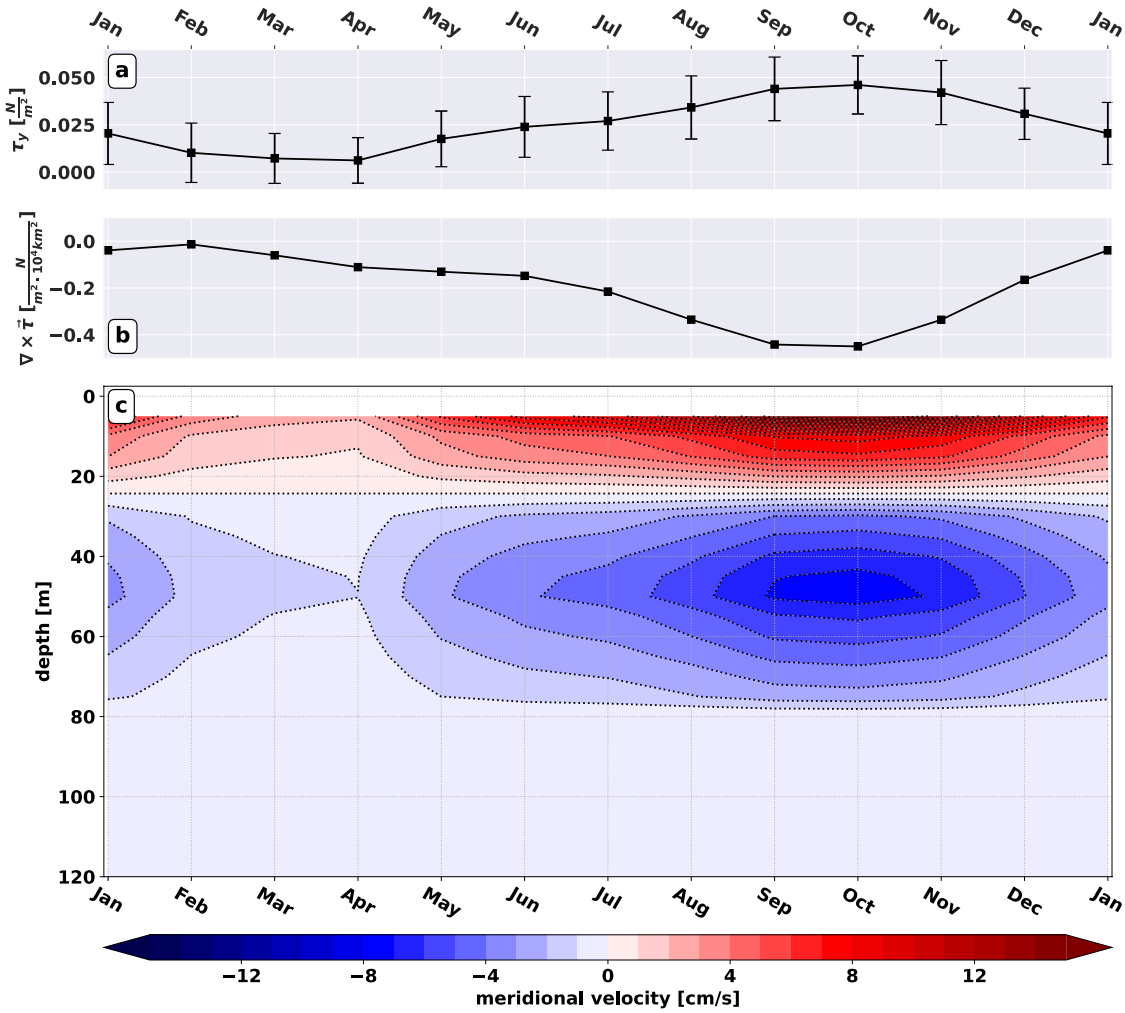

Figure 3. Monthly climatology of (a) mean meridional wind stress (mooring observations) and (b) wind stress curl (Risien & Chelton, 2008) at 0°N, 23°W, error bars indicate one standard deviation and (c) ER meridional velocity field.

coefficient profile due to non-significant regressions were filled by linear interpolation. As already indicated in Figure 2, the meridional wind stress undergoes a distinct seasonal cycle with weak northward or even southward wind stress from February to April and pronounced northward wind stress from September to November (Figure 3a). The curl of the wind stress is persistently negative, yielding southward Sverdrup transport highlighting the analogy to the Indian Ocean ER (Figure 3b). In the upper 22.5 m, ER velocities are directed northward and reach their maximum in October, exceeding 15 cm/s. Further down, ER-associated velocities are southward and weaker in amplitude reaching maximum speeds of 8 cm/s at 50 m in October. Southward velocities cover the depth range from 25 to 80 m (Figure 3c). During this part of the year, the magnitude of both northward surface flow and southward subsurface flow thus represents a significant contribution to the total cross-equatorial flow field, which is otherwise largely determined by the velocity signature of TIWs. Clearly, the ER flow is the dominant process in shaping the seasonal cycle of the meridional velocity at the mooring site (Figure 3c) as it compares well to the monthly climatology of the meridional flow (Figure S3 in Supporting Information S1).

5. Superposition of Tropical Instability Waves and the Equatorial Roll

Assuming a linear superposition, the measured wind can be used to reconstruct and subtract the velocity field of the ER from the meridional flow field. For this, we reconstruct a daily ER velocity field from the vertical regression profile and the PIRATA wind data. At depth, the wind lead is chosen in accordance with the regression analysis (Figure S2a in Supporting Information S1). After subtracting the resulting ER velocity field, the vertical

structure of northward and southward flow phases appears more similar, confirming that TIWs in the central equatorial Atlantic are generally symmetric (Figures 4a and 4b) similarly to the results obtained for TIWs in the equatorial Pacific by Kennant and Flament (2000).

Apart from affecting the meridional flow, the ER adds vertical shear of meridional velocity ($\mathbf{V_z}$). The presence of the EUC and westward flow at the surface above causes elevated levels of vertical shear of zonal velocity ($\boldsymbol{U}_z$) that lead to a state of marginal instability in the upper equatorial thermocline (e.g., Smyth et al., 2013). The mean shear profiles indicate that TIWs provide an additional source of shear to the upper ocean, particularly in the depth range between 50 and 90 m (Figures 4c and 4d). Moreover, the ER adds $\boldsymbol{V}_z$ in the near-surface down to a depth of 40 m during the southward TIW phase and strongly reduces near-surface $\boldsymbol{V}_z$ during the northward TIW phase. This also applies to the depth range between 50 and 100 m, but the effect of the ER on $\boldsymbol{V}_z$ is reduced. This asymmetry in the shear field introduced by the ER is further supported by χ-pod turbulence data at the mooring site (Figures 4e and 4f), providing evidence for enhanced dissipation rates of turbulent kinetic energy (TKE) at 21 and 65 m during periods of pronounced southward flow phases (20–40 cm/s) compared to northward flow phases of similar magnitude. At 21 m the imbalance is not as pronounced as at 65 m due to increased stability of the water column, which might be the result of warm water advection during southward TIW flow, counteracting the enhanced shear. TIW-phase averaged dissipation rates of TKE for all available depth levels and uncertainties are presented in Table S1 in Supporting Information S1. The observed asymmetry should be most intense from August to October when TIWs are still pronounced, and the ER reaches its maximum. Compared to the magnitude of the dominant vertical shear of zonal velocity associated with the EUC and westward flow above, the TIW and ER shear, however, plays a minor role except for the depth range of the EUC core at 75 m with a minimum in $\boldsymbol{U}_z$ and close to the surface where $\boldsymbol{U}_z$ and $\boldsymbol{V}_z$ are similar in magnitude.

6. Summary and Discussion

Variability of the equatorial upper-ocean meridional flow as derived from velocity records of moored observations in the central equatorial Atlantic can be separated into contributions from TIWs and shallow wind-driven meridional baroclinic flow, the ER. The ER, quantified here by linearly regressing meridional wind stress onto meridional velocity from moorings, is characterized by near-surface (<22.5 m depth) northward flow and southward flow between 22.5 and 80 m with a maximum at about 50 m depth. These results provide observational support for previous model studies suggesting that the basic dynamics of the ER are linear and that ER flow is a direct (local) response to the meridional wind stress (Miyama et al., 2003; Pacanowski & Philander, 1981; Wacogne and Pacanowski, 1996). The vertical structure of the ER in the central equatorial Atlantic compares well to observations and model results of the vertical ER structure in the Indian Ocean (e.g., Miyama et al., 2003; Schott et al., 2002; Wang & McPhaden, 2017). Furthermore, as noted in previous studies from the Indian Ocean (Wang & McPhaden, 2017) our findings indicate that the opposing ER-associated meridional flows occur at different densities and involve a net northward heat transport that could be partly balanced by eddy-fluxes (McWilliams & Danabasoglu, 2002). However, the magnitude of the northward heat transport and possible consequences for the mixed-layer heat budget cannot be assessed here.

Once the ER flow is subtracted from the composites of maximum northward and southward intraseasonal flow phases, a near-symmetric meridional flow structure remains that can be ascribed to the signature of northward and southward TIW phases. This symmetry of the TIW phases agrees well with previous studies of TIWs in the equatorial Pacific (Kennan & Flament, 2000).

Shear-driven turbulent mixing in the upper EUC in the Atlantic and Pacific cold tongue is a critical component of the mixed-layer heat budget that drives SST variability and thus affects climate variability (e.g., Hummels et al., 2013; Moum et al., 2013). TIWs enhance the vertical shear of meridional velocity at the equator below the mixed layer. For a train of six TIWs in the Pacific, Inoue et al. (2019) found enhanced vertical shear in the late southern phase and enhanced mixing during the transition from northern to southern flow which they attributed to vortex stretching. In the Atlantic, we show that the seasonal evolution of the ER further modifies the shear field depending on the TIW phase.

With this study, we suggest that the superposition of TIWs and ER has an impact on the strength and seasonal variability of equatorial mixing, thus affecting the mixed-layer heat and freshwater budget. Our results show that the vertical shear of meridional velocity at the equator is not only due to TIWs, but additionally due to the

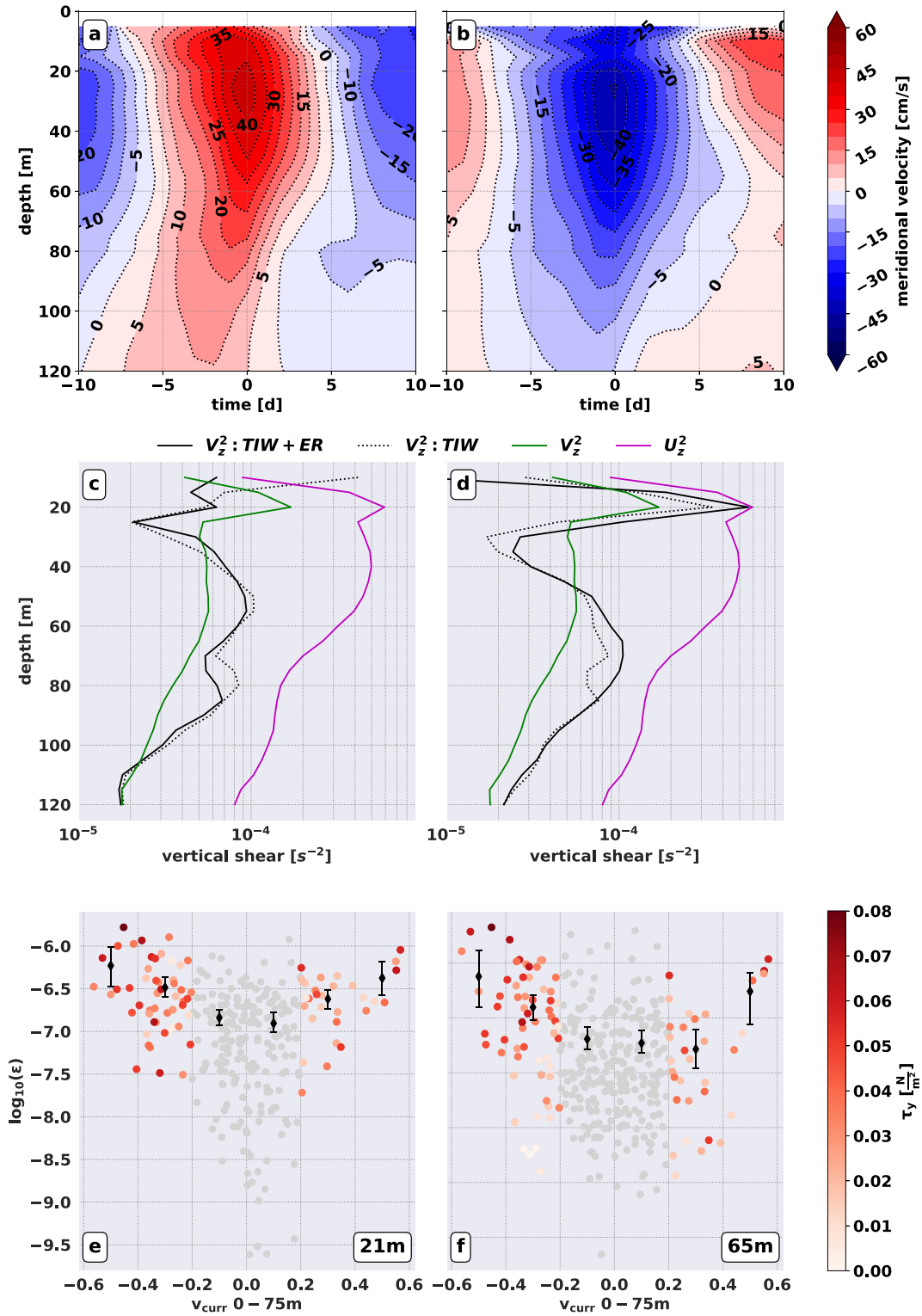

Figure 4. Composite fields of meridional velocity for northward tropical instability waves (TIW) (a) and southward TIW (b) with ER subtracted from each composite member; Composite profiles of vertical shear of meridional velocity for (c) northward and (d) southward phase during maximum meridional flow as well as mean vertical shear of the meridional (green) and zonal (magenta) velocity of the whole recording period. Scatter plots of 0–75 m mean meridional velocity and mean values of turbulent kinetic energy (TKE) dissipation rate (ε) at 21 m (e) and 65 m (f) from the χ-pod data. Black markers indicate mean ε in bins of 0.2 m/s and their 95% confidence intervals. Color represents the meridional wind stress magnitude.

presence of the ER. Thus, the superposition of the ER and the TIWs results in asymmetric vertical shear during north- and southward TIW phases. Indeed, the χ-pod data also show an asymmetry in diapycnal mixing at 21 and 65 m depth which is stronger during southward than during northward TIW phases.

In general, our results suggest that strong southerly wind events combined with southward TIW phases could trigger elevated diapycnal mixing by the combined shear of the EUC, TIWs, and the ER. Due to the overlapping seasonal peaks of TIWs and ER in boreal fall this season might be most favorable for such enhanced mixing events.

Data Availability Statement

The moored velocity data set is available at https://doi.pangaea.de/10.1594/PANGAEA.941042. Buoy wind and χ-pod data can be accessed at https://www.pmel.noaa.gov/tao/drupal/disdel/.

Acknowledgments
This study was funded by EU H2020 under grant agreement 817578 TRIATLAS and 101003470 NextGEMS projects, by the Deutsche Forschungsgemeinschaft and by the Deutsche Bundesministerium fuer Bildung und Forschung as part of the projects NORDATLANTIK (03F0443B) and RACE-Synthese (03F0824C). PIRATA mooring data were provided by the GTMBA Project Office of NOAA/PMEL, which is supported by NOAA's The Global Ocean Monitoring and Observing (GOMO) Program. FP Tuchen is grateful for support from the National Academy of Sciences through an NRC Research Associateship Award held at NOAA's Atlantic Oceanographic and Meteorological Laboratory. Furthermore, PMEL contributed to this study (grant 5271). Mixing measurements and JNM were supported by US National Science Foundation grants 1431518, 2048631. We are greatful for the comments of two anonymous reviewers. Open Access funding enabled and organized by Projekt DEAL.

References

Bourlès, B., Araujo, M., McPhaden, M. J., Brandt, P., Foltz, G. R., Lumpkin, R., et al. (2019). PIRATA: A sustained observing system for tropical Atlantic climate research and forecasting. *Earth and Space Science*, *6*(4), 577–616. https://doi.org/10.1029/2018EA000428

Brandt, P., Hahn, J., Schmidtko, S., Tuchen, F. P., Kopte, R., Kiko, R., et al. (2021). Atlantic equatorial undercurrent intensification counteracts warming-induced deoxygenation. *Nature Geoscience*, *14*(5), 278–282. https://doi.org/10.1038/s41561-021-00716-1

Brandt, P., Schott, F. A., Provost, C., Kartavtseff, A., Hormann, V., Bourlès, B., & Fischer, J. (2006). Circulation in the central equatorial Atlantic: Mean and intraseasonal to seasonal variability. *Geophysical Research Letters*, *33*(7), L07609. https://doi.org/10.1029/2005GL025498

Fratantoni, D. M., Johns, W. E., Townsend, T. L., & Hurlburt, H. E. (2000). Low-latitudecirculation and mass transport pathways in a model of the tropical Atlantic Ocean. *Journal of Physical Oceanography*, *30*(8), 1944–1966. https://doi.org/10.1175/1520-0485(2000)030<1944:LLCAMT>2.0.CO;2

Grodsky, S. A., Carton, J. A., & Nigam, S. (2003). Near surface westerly wind jet in the Atlantic ITCZ. *Geophysical Research Letters*, *30*(19), 1–4. https://doi.org/10.1029/2003GL017867

Grodsky, S. A., Carton, J. A., Provost, C., Servain, J., Lorenzzetti, J. A., & McPhaden, M. J. (2005). Tropical instability waves at 0°N, 23°W in the Atlantic: A case study using pilot research moored array in the tropical Atlantic (PIRATA) mooring data. *Journal of Geophysical Research*, *110*(C8), C08010. https://doi.org/10.1029/2005JC002941

Holmes, R., & Thomas, L. (2015). The modulation of equatorial turbulence by tropical instability waves in a regional ocean model. *Journal of Physical Oceanography*, *45*(4), 1155–1173. https://doi.org/10.1175/JPO-D-14-0209.1

Hummels, R., Dengler, M., & Bourlès, B. (2013). Seasonal and regional variability of upper ocean diapycnal heat flux in the Atlantic cold tongue. *Progress in Oceanography*, *111*, 52–74. https://doi.org/10.1016/j.pocean.2012.11.001

Inoue, R., Lien, R. C., Moum, J. N., Perez, R. C., & Gregg, M. C. (2019). Variations of equatorial shear, stratification, and turbulence within a tropical instability wave cycle. *Journal of Geophysical Research: Oceans*, *124*(3), 1858–1875. https://doi.org/10.1029/2018JC014480

Jochum, M., Malanotte-Rizzoli, P., & Busalacchi, A. (2004). Tropical instability waves in the Atlantic Ocean. *Ocean Modelling*, *7*(1–2), 145–163. https://doi.org/10.1016/S1463-5003(03)00042-8

Kelly, B. G., Meyers, S. D., & O'Brien, J. J. (1995). On a generating mechanism for Yanaiwaves and the 25-day oscillation. *Journal of Geophysical Research*, *100*(C6), 10589–10612. https://doi.org/10.1029/94JC02911

Kennan, S. C., & Flament, P. J. (2000). Observations of a tropical instability vortex. *Journal of Physical Oceanography*, *30*(9), 2277–2301. https://doi.org/10.1175/1520-0485(2000)030<2277:OOATIV>2.0.CO;2

Körner, M., Claus, M., Brandt, P., & Tuchen, F. P. (2022). Sources and pathways of intraseasonal meridional kinetic energy in the equatorial Atlantic Ocean. *Journal of Physical Oceanography*. https://doi.org/10.1175/JPO-D-21-0315.1

Liu, C., Fang, L., Köhl, A., Liu, Z., Smyth, W. D., & Wang, F. (2019). The subsurface mode tropical instability waves in the equatorial Pacific Ocean and their impacts on shear and mixing. *Geophysical Research Letters*, *46*(21), 12270–12278. https://doi.org/10.1029/2019GL085123

Mayer, D. A., & Weisberg, R. H. (1993). A description of COADS surface meteorological fields and the implied sverdrup transports for the Atlantic Ocean from 30°S to 60°N. *Journal of Physical Oceanography*, *23*(10), 2201–2221. https://doi.org/10.1175/1520-0485(1993)023<2201:ADOCSM>2.0.CO;2

McCreary, J. P., Jr., & Yu, Z. (1992). Equatorial dynamics in a 212-layer model. *Progress in Oceanography*, *29*(1), 61–132. https://doi.org/10.1016/0079-6611(92)90003-I

McWilliams, J. C., & Danabasoglu, G. (2002). Eulerian and eddy-induced meridional overturning circulations in the tropics. *Journal of Physical Oceanography*, *32*(7), 2054–2071. https://doi.org/10.1175/1520-0485(2002)032<2054:EAEIMO>2.0.CO;2

Miyama, T., McCreary, J. P., Jr., Jensen, T. G., Loschnigg, J., Godfrey, S., & Ishida, A. (2003). Structure and dynamics of the Indian-ocean crossequatorial cell. *Deep Sea Research Part II: Topical Studies in Oceanography*, *50*(12–13), 2023–2047. https://doi.org/10.1016/S0967-0645(03)00044-4

Moum, J., Lien, R.-C., Perlin, A., Nash, J., Gregg, M., & Wiles, P. (2009). Sea surface cooling at the equator by subsurface mixing in tropical instability waves. *Nature Geoscience*, *2*(11), 761–765. https://doi.org/10.1038/ngeo657

Moum, J. N., Hughes, K. G., Shroyer, E. L., Smyth, W. D., Cherian, D., Warner, S. J., et al. (2022). Deep cycle turbulence in Atlantic and Pacific cold tongues. *Geophysical Research Letters*, *49*(8), e2021GL097345. https://doi.org/10.1029/2021GL097345

Moum, J. N., Perlin, A., Nash, J. D., & McPhaden, M. J. (2013). Seasonal sea surface cooling in the equatorial Pacific cold tongue controlled by ocean mixing. *Nature*, *500*(7460), 64–67. https://doi.org/10.1038/nature12363

Pacanowski, R., & Philander, S. (1981). Parameterization of vertical mixing in numerical models of tropical oceans. *Journal of Physical Oceanography*, *11*(11), 1443–1451. https://doi.org/10.1175/1520-0485(1981)011<1443:POVMIN>2.0.CO;2

Perez, R. C., Foltz, G. R., Lumpkin, R., & Schmid, C. (2019). Direct measurements of upper ocean horizontal velocity and vertical shear in the tropical North Atlantic at 4N, 23W. *Journal of Geophysical Research: Oceans*, *124*(6), 4133–4151. https://doi.org/10.1029/2019JC015064

Perez, R. C., Hormann, V., Lumpkin, R., Brandt, P., Johns, W. E., Hernandez, F., et al. (2014). Mean meridional currents in the central and eastern equatorial Atlantic. *Climate Dynamics*, *43*(11), 2943–2962. https://doi.org/10.1007/s00382-013-1968-5

Risien, C. M., & Chelton, D. B. (2008). A global climatology of surface wind and wind stress fields from eight years of QuikSCAT scatterometer data. *Journal of Physical Oceanography*, *38*(11), 2379–2413. https://doi.org/10.1175/2008JPO3881.1

Schott, F. A., Dengler, M., & Schoenefeldt, R. (2002). The shallow overturning circulation of the Indian Ocean. *Progress in Oceanography*, *53*(1), 57–103. https://doi.org/10.1016/S0079-6611(02)00039-3

Schott, F. A., Xie, S.-P., & McCreary, J. P., Jr. (2009). Indian ocean circulation and climate variability. *Reviews of Geophysics*, *47*(1), RG1002. https://doi.org/10.1029/2007RG000245

Smyth, W., Moum, J., Li, L., & Thorpe, S. (2013). Diurnal shear instability, the descent of the surface shear layer, and the deep cycle of equatorial turbulence. *Journal of Physical Oceanography*, *43*(11), 2432–2455. https://doi.org/10.1175/JPO-D-13-089.1

Specht, M. S., Jungclaus, J., & Bader, J. (2021). Identifying and characterizing subsurface tropical instability waves in the Atlantic Ocean in simulations and observations. *Journal of Geophysical Research: Oceans*, *126*(10), e2020JC017013. https://doi.org/10.1029/2020JC017013

Tuchen, F. P., Brandt, P., Claus, M., & Hummels, R. (2018). Deep intraseasonal variability in the central equatorial Atlantic. *Journal of Physical Oceanography*, *48*(12), 2851–2865. https://doi.org/10.1175/JPO-D-18-0059.1

Tuchen, F. P., Brandt, P., Hahn, J., Hummels, R., Krahmann, G., Bourlès, B., et al. (2022). Two decades of full-depth current velocity observations from a moored observatory in the central equatorial Atlantic at 0°N, 23°W. *Frontiers in Marine Science*, *9*, 910979. https://doi.org/10.3389/fmars.2022.910979

von Schuckmann, K., Brandt, P., & Eden, C. (2008). Generation of tropical instability waves in the Atlantic Ocean. *Journal of Geophysical Research*, *113*(C8), C08034. https://doi.org/10.1029/2007JC004712

Wacongne, S., & Pacanowski, R. (1996). Seasonal heat transport in a primitive equations model of the tropical Indian Ocean. *Journal of Physical Oceanography*, *26*(12), 2666–2699. https://doi.org/10.1175/1520-0485(1996)026<2666:SHTIAP>2.0.CO;2

Wang, Y., & McPhaden, M. J. (2017). Seasonal cycle of cross-equatorial flow in the central Indian Ocean. *Journal of Geophysical Research: Oceans*, *122*(5), 3817–3827. https://doi.org/10.1002/2016JC012537

Wenegrat, J. O., & McPhaden, M. J. (2015). Dynamics of the surface layer diurnal cycle in the equatorial Atlantic Ocean (0°, 23°W). *Journal of Geophysical Research: Oceans*, *120*(1), 563–581. https://doi.org/10.1002/2014JC010504

Wenegrat, J. O., McPhaden, M. J., & Lien, R.-C. (2014). Wind stress and near-surface shear in the equatorial Atlantic Ocean. *Geophysical Research Letters*, *41*(4), 1226–1231. https://doi.org/10.1002/2013GL059149

References From the Supporting Information

Efron, B. (1982). *The Jackknife, the bootstrap and other resampling plans* (p. 92). Society for Industrial and Applied Mathematics.

Moum, J. N., & Nash, J. D. (2009). Mixing measurements on an equatorial ocean mooring. *Journal of Atmospheric Oceanic Technology*, *26*(2), 317–336. https://doi.org/10.1175/2008JTECHO617.1

Perlin, A., & Moum, J. N. (2012). Comparison of thermal dissipation rate estimates from moored and profiling instruments at the equator. *Journal of Atmospheric Oceanic Technology*, *29*(9), 1347–1362. https://doi.org/10.1175/JTECH-D-12-00019.1